N91-17098

A Technique for Optimal Temperature Estimation for Modeling Sunrise/Sunset Thermal Snap Disturbance Torque

D. F. Zimbelman*
C. J. Dennehy†
R. V. Welch‡
Fairchild Space Company
Fairchild Space Systems Division
Germantown, Maryland
U.S.A. 20874-1181

G. H. Born§
Colorado Center for Astrodynamics Research
University of Colorado
Boulder, Colorado
U.S.A. 80309-0431

ABSTRACT

This paper describes a predictive temperature estimation technique which can be used to drive a model of the Sunrise/Sunset thermal "snap" disturbance torque experienced by low Earth orbiting spacecraft. The twice per orbit impulsive disturbance torque is attributed to vehicle passage in and out of the Earth's shadow cone (umbra), during which, large flexible appendages undergo rapidly changing thermal conditions. Flexible members, in particular solar arrays, experience rapid cooling during umbra entrance (Sunset) and rapid heating during exit (Sunrise). The thermal "snap" phenomena has been observed during normal on-orbit operations of both the LANDSAT-4 satellite and the Communications Technology Satellite (CTS). Thermal "snap" has also been predicted to be a dominant source of error for the TOPEX satellite.

The fundamental equations used to model the Sunrise/Sunset thermal "snap" disturbance torque for a typical solar array like structure will be described. For this derivation the array is assumed to be a thin, cantilevered beam. The time varying thermal gradient is shown to be the driving force behind predicting the thermal "snap" disturbance torque and therefore motivates the need for accurate estimates of temperature. This paper will highlight the development of a technique to optimally estimate appendage surface temperatures. The objective analysis method used is structured on the Gauss-Markov Theorem and provides an optimal temperature estimate at a prescribed location given data from a distributed thermal sensor network. The optimally estimated surface temperatures could then be used to compute the thermal gradient across the body. The estimation technique is demonstrated using a typical satellite solar array.

---

*Engineer, GN&C Department. Graduate Student, Colorado Center for Astrodynamics Research/University of Colorado.

†Section Manager, GN&C Department.

‡Senior Director, GN&C Department.

§Director, Colorado Center for Astrodynamics Research/University of Colorado. Professor, Aerospace Engineering Sciences.

INTRODUCTION

In the early 1980's, an unexpected perturbation was experienced by the LANDSAT-4 and 5 satellites. An anomously large, twice per orbit disturbance was observed in the flight data during normal on-orbit operations. An example of this disturbance is illustrated in Figures 1 and 2 which show the LANDSAT-4 roll and yaw axes derived rate telemetry data, respectively, over one orbital period. An inspection of Figures 1 and 2 reveals that the roll and yaw controlled response of the vehicle exhibits an impulsive velocity in one direction immediately followed by a similar motion in the opposite direction, and finally proceeded by a decaying step of the initial sign. There is minimal coupling present in the pitch axis data which indicates the disturbance is primarily distributed between the roll and yaw axes. The perturbation shown in Figures 1 and 2 has been correlated with the spacecraft's entrance (sunset) and exit (sunrise) to the eclipsed region of the orbit plane. During penumbral transitions, the vehicle undergoes rapidly changing thermal conditions which result in a thermally induced bending motion of the large single solar array. If the snaping or bending motion occurs at a non-constant rate a disturbance torque is generated about the hinged axis of the array, which is then transferred back onto the vehicle core-body. This concept is illustrated in Figure 3. This thermally induced disturbance, referred to as Thermal "snap" or Thermal Elastic Shock (TES), has also been observed during the three-axis stabilized operation of the Communications Technology Satellite (CTS), but to a much lesser degree. The difference in perturbation magnitude was a result of the differences between the two spacecraft designs. The TES disturbance is most pronounced for asymmetric satellite configurations, such as the single-wing LANDSAT vehicles. Satellites possesing a dual-wing array design, such as CTS, are significantly less affected by TES since the motion of both arrays tends to be self-compensating. However, a single array configuration is typically required to provide an unobstructed radiator view of cold space for proper thermal control of mission sensor payload instruments.

The significant attitude excursions experienced by the LANDSAT vehicles in response to the TES disturbance have aroused considerable concern for future satellite missions. This is especially true for the Upper Atmospheric Research Satellite (UARS) and the TOPography EXperiment (TOPEX) satellite since both vehicles utilize LANDSAT heritage. In particular, the TES disturbance has been predicted to be a dominant source of attitude perturbation for the TOPEX spacecraft [*Dennehy et al.*, 1988]. *Dennehy et al.* [1990] have analyzed the attitude pointing performance of the TOPEX spacecraft when subjected to the TES disturbance. Their analysis found that the TES disturbance was large enough to cause the TOPEX spacecraft to temporarily exceed its Normal Mission Mode (NMM) attitude pointing requirements. Consequently, some degraded performance of the primary scientific instrument will be experienced for a brief period of time. Thus, for TOPEX and other future satellites, a need is established to determine the on-orbit magnitude of the TES disturbance in order to compensate science data taken during degraded attitude periods. Temperature data could be used in one of two ways to counteract the TES disturbance. The first methodology would utilize the temperature data in an on-board implementation to provide adjustments in order to accommodate the TES disturbance torque. The second procedure would employ the use of temperature telemetry data to drive a TES disturbance model so *a postori* attitude reconstruction could be performed on the ground.

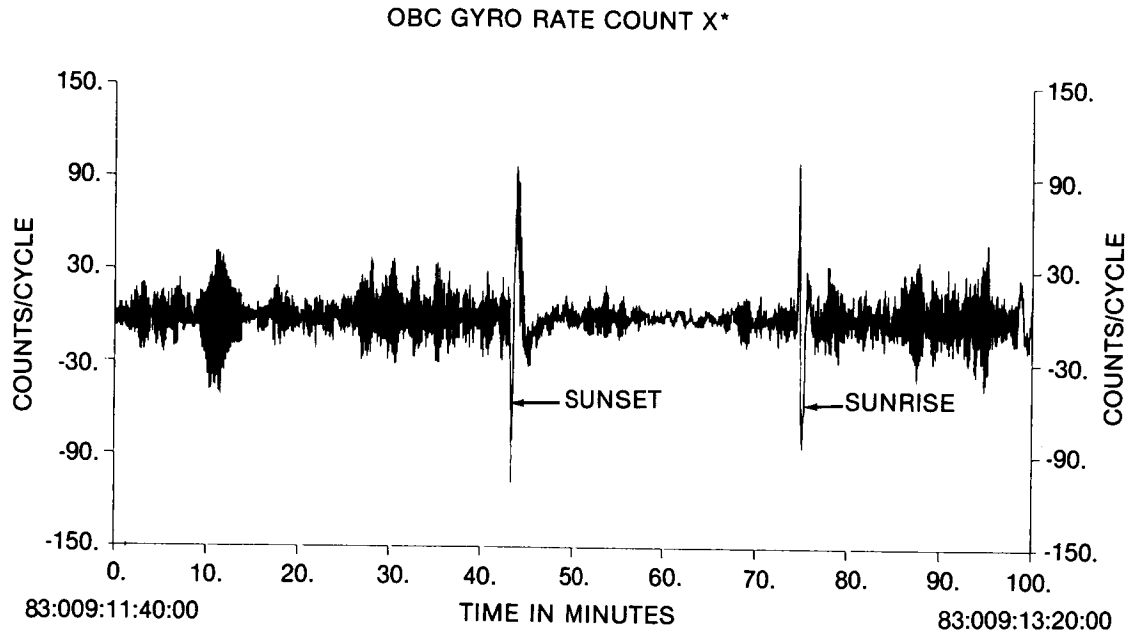

*Where: 1 count = 0.05 Arseconds, and 1 cycle = 0.512 Seconds

S-019.528

Figure 1: On-Orbit LANDSAT-4 Sunrise/Sunset Disturbance (Roll Axis)

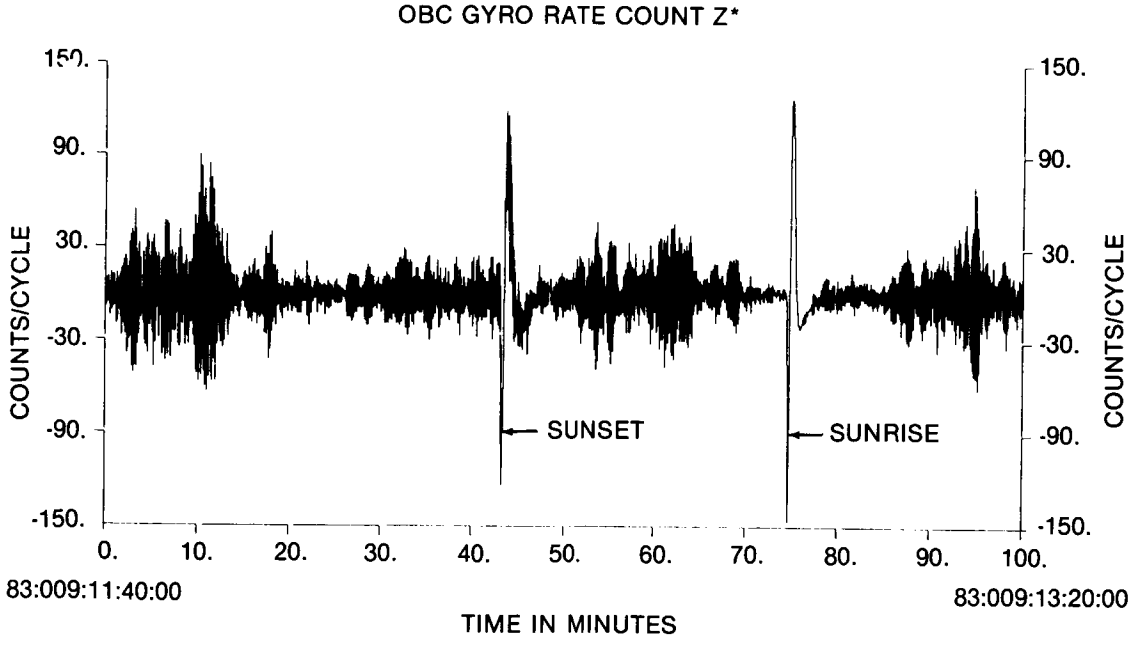

*Where: 1 count = 0.05 Arcseconds and, 1 cycle = 0.512 Seconds

S-019.529

Figure 2: On-Orbit LANDSAT-4 Sunrise/Sunset Disturbance (Yaw Axis)

TES DISTURBANCE MODEL

A mathematical representation for the TES disturbance torque for a typical satellite solar array has been developed by *Dennehy et al.* [1990]. This model is essentially the second time derivative of the array inertia multiplied by the angle through which the array bends. For the TES disturbance model, the solar array is assumed to be a thin, cantilevered beam with mass M and length L. The general form of the disturbance torque is expressed as [*Dennehy et al.*, 1990]:

$$T_b = 2\dot{f}(t-\tau)\dot{u}(t-\tau) + \ddot{f}(t-\tau)u(t-\tau) \tag{1}$$

where $u(t-\tau)$ is a unit *step* function defined as:

$$u(t-\tau) = \begin{cases} 0 & \text{if } t < \tau \\ 1 & \text{if } t \geq \tau \end{cases} \tag{2}$$

and $\dot{u}(t-\tau)$ is a *Dirac* function described as:

$$\dot{u}(t-\tau) = \begin{cases} 1 & \text{if } t = \tau \\ 0 & \text{otherwise} \end{cases} \tag{3}$$

If the array is broken into n pieces, where n is sufficiently large, then a general expression for the function $f(t-\tau)$ can be formulated as:

$$f(t-\tau) = \sum_{i=1}^{n} \left[\frac{l_i m_i d}{\alpha_{cte}\Delta T}\left(1 - \cos\left[\frac{l_i \alpha_{cte}\Delta T}{d}\right]\right)\right] \tag{4}$$

where

d $\equiv$ thickness of the array
τ $\equiv$ point of umbra entrance or exit
ΔT $\equiv$ thermal gradient across the array
α_{cte} $\equiv$ material coefficient of thermal expansion

The parameters l_i and m_i are determined using the following relations:

$$l_i = \frac{L}{n}\left(i - \frac{1}{2}\right) \tag{5}$$

$$m_i = \frac{M}{n} \tag{6}$$

Substituting Equations 2, 3 and 4 into Equation 1 yields a standard expression for the TES disturbance torque:

$$T_b = \begin{cases} 0 & \text{if } t < \tau \\ T_\varsigma + \frac{\ddot{\Delta T} H_b}{\Delta T} - \frac{2\dot{\Delta T} H_b}{\Delta T} & \\ + \sum_{i=1}^{n} \frac{l_i^3 m_i \alpha_{cte} \dot{\Delta T}^2}{d\Delta T} \cos\left[\frac{l_i \alpha_{cte}\Delta T}{d}\right] & \text{if } t \geq \tau \end{cases} \tag{7}$$

where

$$T_\zeta = \begin{cases} 2H_b & \text{if } t = \tau \\ 0 & \text{if } t > \tau \end{cases} \tag{8}$$

and H_b is the array momentum given as:

$$H_b = \begin{cases} 0 & \text{if } t < \tau \\ \sum_{i=1}^{n} -\frac{l_i m_i d\dot{\Delta T}}{\alpha_{cte}\Delta T^2}(1 - \cos[\frac{l_i \alpha_{cte}\Delta T}{d}] & \\ -\frac{l_i \alpha_{cte}\Delta T}{d}\sin[\frac{l_i \alpha_{cte}\Delta T}{d}]) & \text{if } t \geq \tau \end{cases} \tag{9}$$

It is apparent from Equations 7, 8 and 9 that the TES disturbance torque is a function of not only the thermal gradient across the array, but is also dependent on the first and second time derivatives of the thermal gradient, $\dot{\Delta T}$ and $\ddot{\Delta T}$. Thus in order to predict the magnitude of the TES disturbance using the mathematical model, an array temperature gradient profile is necessary.

OPTIMAL TEMPERATURE ESTIMATION

The dependence of the TES disturbance torque model on the successive derivatives of the thermal gradient motivates the need for accurate temperature determination. The thermal response of a solar array may be predicted using numerical techniques such as those presented in *Dennehy et al.* [1990]. Such methods include using the Thermal Radiation Analysis SYStem (TRASYS) and the Systems Improved Numerical Differencing Analyzer (SINDA) software packages, as well as solving the one-dimensional heat equation

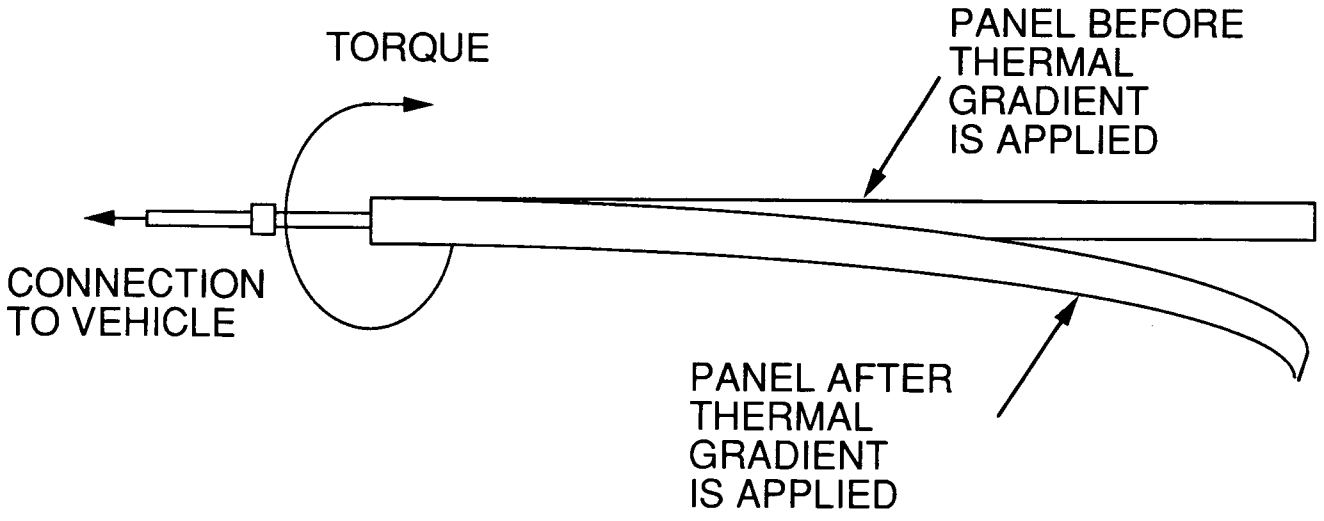

Figure 3: Solar Array Structural Deflection Due to Applied Thermal Gradient

using finite difference approximations. However, to measure the true thermal response of a solar array, thermal sensors are used during on-orbit spacecraft operation. Thermal sensors utilized for spaceflight applications include thermisters and platinum resistance thermometers (PRT). Thermisters are accurate to about $\pm 4^{\circ}C$ while the accuracy of a PRT is approximately $\pm 1^{\circ}C$. If a distributed network of thermal sensors exists on each surface of the array, as illustrated in Figure 4 for the front panel, a measurement of the surface temperatures at those prescribed locations is obtained. It would be nice to use all the available surface temperature information to estimate the array surface temperature at a desired location. Thus a technique, based on the Gauss-Markov Theorem, is described to optimally estimate array surface temperatures. Then once the temperature estimate for each surface is determined, the thermal gradient may be predicted by differencing the front and back surface temperatures at a consistant specified location.

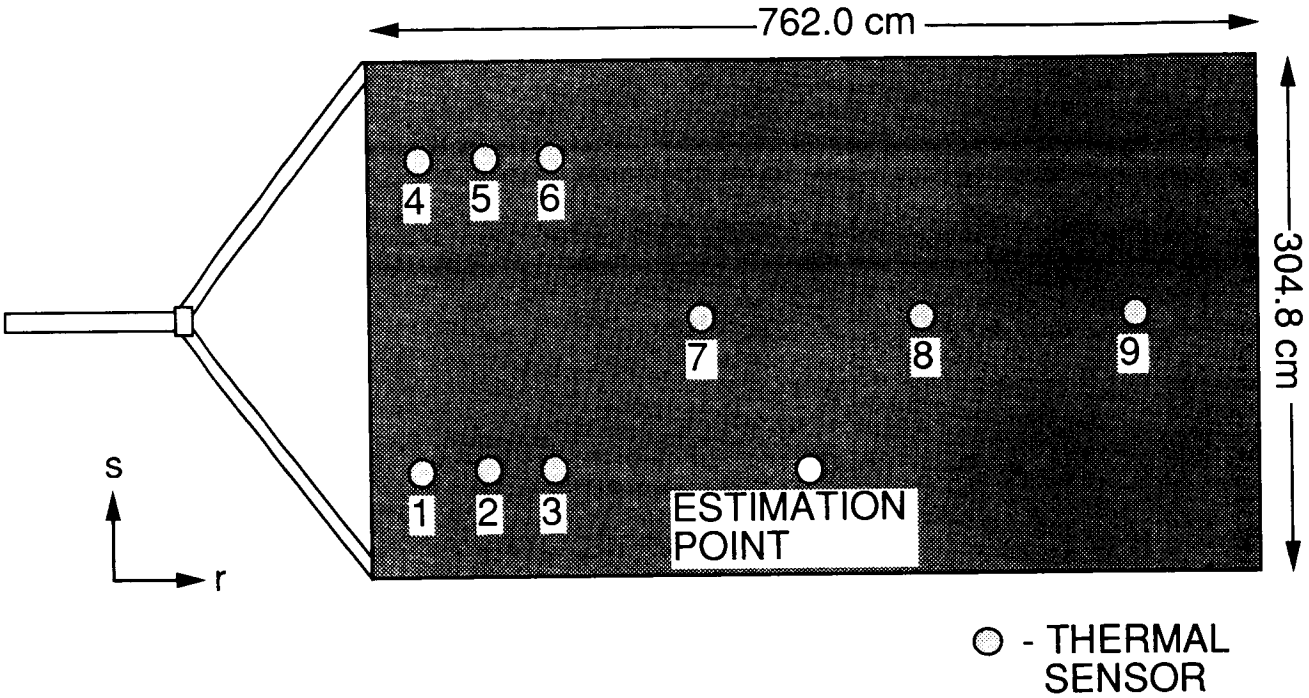

Figure 4: 9-Element Distributed Thermal Sensor Network on a Typical Solar Array (Front Surface)

The Gauss-Markov theorem provides a linear minimum mean square estimate of a vector x with n components given a set of m observations, Θ. The estimator, given by *Liebelt* [1967], is stated as follows:

$$\hat{x} = C_{x\Theta} C_{\Theta}^{-1} \Theta \tag{10}$$

where

$$\begin{aligned} C_{x\Theta} &\equiv E(x\Theta^T)\ (n \times m\ matrix) \\ C_{\Theta} &\equiv E(\Theta\Theta^T)\ (m \times m\ matrix) \\ E &\equiv \text{expected value operator} \end{aligned}$$

The error matrix associated with the estimate of x is given as [*Liebelt*, 1967]:

$$C_e = C_x - C_{x\Theta} C_{\Theta}^{-1} C_{x\Theta}^T \tag{11}$$

with

$$C_x \equiv E(xx^T)\ (n \times n\ matrix)$$

If the expected value of the estimate, $E(\hat{x})$, is equal to x (i.e. the average of the estimate is equal to the true value) then $\hat{x}$ is a linear minimum variance unbiased estimate and C_e is the covariance matrix of the estimate. The error gives a indication of how the estimate is dispersed from the true value. If the error is small then the estimate approaches the true value.

Equations 10 and 11 form the basis of the optimal estimation method developed by *Bretherton et al.* [1976]. For their analysis, the Gauss-Markov theorem was utilized to estimate the value of a two-dimensional scaler variable at a specified location given measurement data at a limited number of positions. A linear form of the observations is assumed and can be expressed as:

$$\varphi_i = \Theta(r,s) + \epsilon_i \tag{12}$$

for $i = 1, ..., N$ where

$$\begin{aligned} \varphi_i &\equiv i^{th} \text{ measurement} \\ \epsilon_i &\equiv i^{th} \text{ measurement error} \\ N &\equiv \text{total number of observations} \\ \Theta(r,s) &\equiv \text{scaler variable at position } (r,s) \end{aligned}$$

Furthermore, the assumption is made that the measurement errors are uncorrelated and independent of φ. Under these assumptions, *Bretherton et al.* [1976] applied the Gauss-Markov theorem, Equations 10 and 11, to obtain the resulting estimation equation given as follows:

$$\hat{\Theta} = \bar{\Theta} + \sum_{i=1}^{N} C_{xi}[\sum_{j=1}^{N} A_{ij}^{-1}(\varphi_j - \bar{\Theta})] \tag{13}$$

where

$$\begin{aligned} \bar{\Theta} &\equiv \text{estimated mean of the observations} \\ A_{ij} &\equiv \text{covariance between all pairs of observations} \\ C_{xi} &\equiv \text{covariance between the estimate and the } i^{th} \text{ observation} \end{aligned}$$

and the associated error matrix, C_e given as:

$$C_e = C_x - \sum_{i=1}^{N}\sum_{j=1}^{N} C_{xi}C_{xj}A_{ij}^{-1} \tag{14}$$

The estimated mean is computed under the condition that the sum of the weighted measurements is zero and is determined by the following equation [*Bretherton et al.*, 1976]:

$$\bar{\Theta} = \frac{\sum_{i=1}^{N}\sum_{j=1}^{N} A_{ij}^{-1}\varphi_j}{\sum_{i=1}^{N}\sum_{j=1}^{N} A_{ij}^{-1}} \tag{15}$$

Equations 13, 14 and 15 will be used to provide an optimal estimate of a solar array temperature at a prescribed location and the error associated with the estimate in order to demonstrate the estimation technique.

APPLICATION

The key to implementing the optimal estimation technique is the determination of both the C_x matrix and an analytic weighting function to scale the variance of the data. The weighting function is necessary to compute numerical values for the C_{xi} and A_{ij} matrices. The C_x matrix is generally unknown but can be approximated by the variance of the given data set. The numerical computation of C_x for this analysis was performed using the following equation [*Bretherton et al., 1976*]:

$$C_x = \sigma_\varphi^2 + \frac{(1 - \sum_{i=1}^{N}\sum_{j=1}^{N} C_{xi}A_{ij}^{-1})^2}{\sum_{i=1}^{N}\sum_{j=1}^{N} A_{ij}^{-1}} \tag{16}$$

where σ_φ is the standard deviation of the measurement data given as:

$$\sigma_\varphi = \sqrt{\frac{\sum_{i=1}^{N}(\varphi_i - \bar{\varphi})^2}{N-1}} \tag{17}$$

with

$$\bar{\varphi} = \frac{\sum_{i=1}^{N}\varphi_i}{N} \tag{18}$$

The last term on the right hand side of Equation 16 accounts for uncertainties associated with the estimated mean.

A weighting function was selected, for this study, to weight the measurements according to their spatial location with respect to one another and to the desired position of the estimate. This type of weighting function can be used as a first cut statistical model given no *a priori* knowledge of the data statistics. The estimation technique can, however, easily accommodate more complex statistical models if desired. An analytical expression for the weighting function is given as:

$$W_{ij} = 0.2(\gamma - \bar{r_{ij}}^2 - \bar{s_{ij}}^2)\exp^{-\sqrt{\bar{r_{ij}}^2 + \bar{s_{ij}}^2}} \tag{19}$$

where

γ $\equiv$ measurement degradation factor

$\bar{r_{ij}}$ $\equiv$ scaling parameter between the i^{th} and j^{th} observations in the r direction

$\bar{s_{ij}}$ $\equiv$ scaling parameter between the i^{th} and j^{th} observations in the s direction

The parameter γ is introduced to change the quality of the observations. If γ is set equal to 5.0 then a maximum correlation of 1.0 will exist when the condition $i = j$ is satisfied in

Equation 19. As γ linearly decreases, the maximum attainable correlation also decreases in a linear fashion. The scaling parameters, $\bar{r_{ij}}$ and $\bar{s_{ij}}$, are calculated using the following equations:

$$\bar{r_{ij}} = \frac{r_i - r_j}{r_{scale}} \tag{20}$$

and

$$\bar{s_{ij}} = \frac{s_i - s_j}{s_{scale}} \tag{21}$$

The variables r_{scale} and s_{scale} can be specified to determine an effective range of data influence (decorrelation scale) or set to the dimensions of the spatial area over which the measurements are confined. For the present study, the latter condition is used. The variables r_i and s_i denote the spatial location of the i^{th} observation location while the variables r_j and s_j indicate the spatial position of the j^{th} point. Thus a spatially weighted covariance can be computed between the point of estimation and the measurements, C_{xi}, and between the observations themselves, A_{ij}, given the weighting function. The calculation of C_{xi} can be expressed by:

$$C_{xi} = W_{xi}\sigma_\varphi^2 \tag{22}$$

where the subscript x is used to denote the desired location, (r_x, s_x), of the estimate, while the weighted observation matrix, A_{ij}, is determined from the following equation:

$$A_{ij} = W_{ij}\sigma_\varphi^2 + \sigma_\epsilon^2\delta_{ij} \tag{23}$$

where δ_{ij} is the *Kronecker* delta function expressed as:

$$\delta_{ij} = \begin{cases} 0 & \text{if i} \neq \text{j} \\ 1 & \text{if i} = \text{j} \end{cases} \tag{24}$$

and σ_ϵ the standard deviation of the error.

The one drawback of using this technique is the inversion of the observation covariance matrix, A_{ij}. If a large number of observations exist then the dimension of the covariance matrix becomes cumbersome and hard to numerically invert. However, to speed the nu-

Table 1: Thermal Sensor Locations and Temperature Measurements for Cases 1-3

Sensor No.	Sensor Position		Temperature $°C$		
	r (cm)	s (cm)	Case 1	Case 2 (Thermister)	Case 3 (PRT)
1	31.75	76.2	72.8795	75.6214	73.8198
2	95.25	76.2	72.9475	75.1302	72.4815
3	158.75	76.2	72.9530	69.0273	73.5481
4	31.75	228.6	72.8510	76.0959	73.4943
5	95.25	228.6	72.9433	70.5750	72.3178
6	158.75	228.6	72.9525	71.1157	73.8453
7	285.75	152.4	72.9534	72.4241	72.9780
8	476.25	152.4	72.9534	72.7547	72.4672
9	666.75	152.4	72.9534	72.8162	72.7367

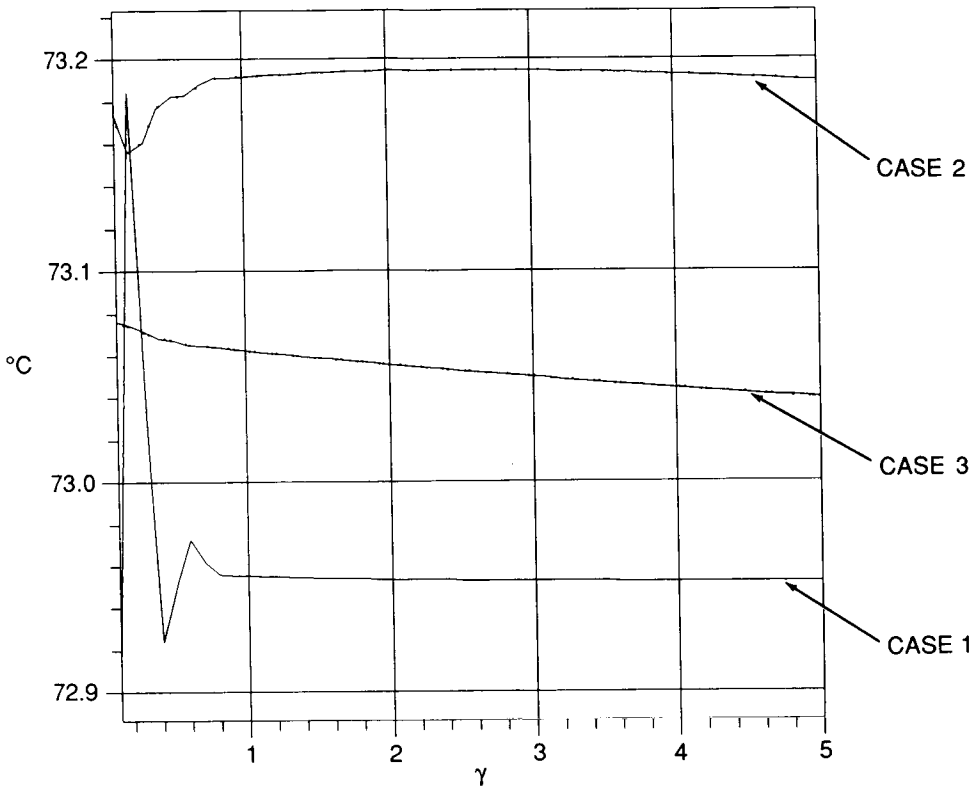

Figure 5: Temperature Estimates Versus Measurement Degradation Factor for Cases 1-3

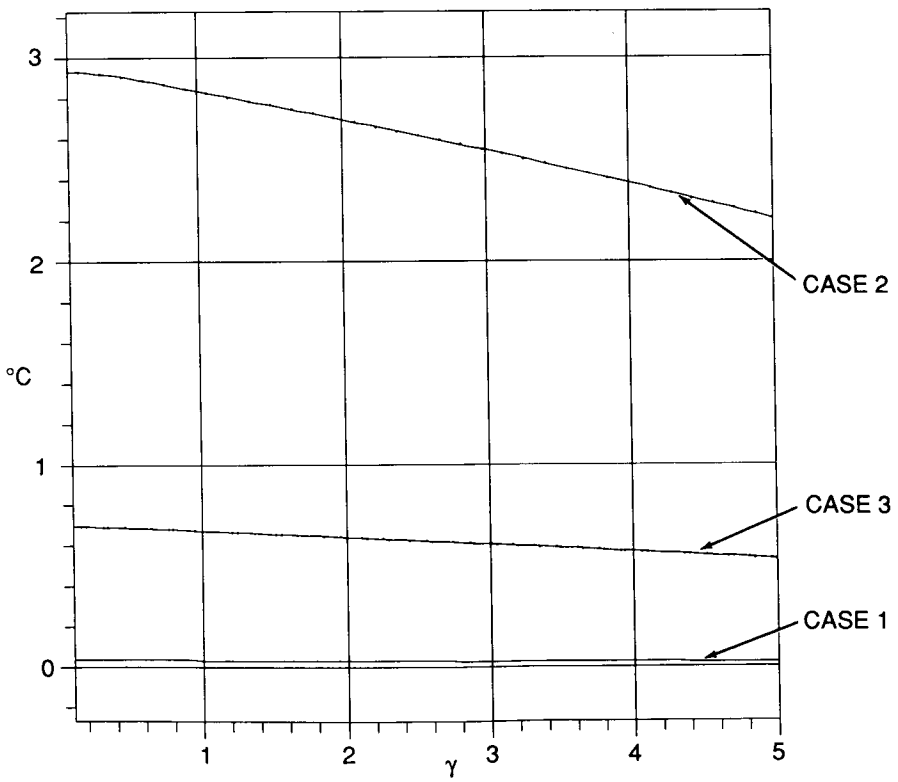

Figure 6: Standard Deviation of Temperature Estimates Versus Measurement Degradation Factor for Cases 1-3

merical inversion process, the order of the covariance matrix could be reduced, keeping only those observations having a correlation value above a specified limit.

RESULTS

For this study, the arrangement of the thermal sensors on a typical solar array front surface, labeled 1 through 9 as shown in Figure 4, represent the spatial location of the temperature observations. The length (762.0 cm) and width (304.8 cm) of the array represent the spatial area scales, r_{scale} and s_{scale} respectively. To demonstrate the technique, temperature measurements at the nine locations, all at a single point in time, are used. The factor γ is set equal to 5.0 to provide a maximum correlation of 1.0. The technique is first used with data that is assumed true with no measurement error, e.g. $\epsilon_i = 0$. Thus the error matrix will represent the covariance of the unbiased estimate. The temperature data and the locations of the thermal sensors are listed in Table 1 under the Case 1 heading. The prescribed point of estimation is positioned at (381,50.8) cm for this and all examples. Applying the technique, the computed estimate is 72.9523°C with a standard deviation of 0.023°C. The estimated temperature is consistant with the observed data and the standard deviation of 0.023°C represents a small deviation from the true temperature at the estimation point. A second example is illustrated by corrupting the true temperature measurements with error. In one case the sensors are considered to be thermisters and in another the PRT sensor is used. The standard deviation of the error is assumed to be 4°C for the thermister and 1°C for the PRT. Case 2 shows the thermister simulated temperature data and Case 3 represents the PRT data as shown in Table 1. The temperature estimates for the thermister and PRT data are 73.1893°C and 73.0396°C with standard deviations of 2.205°C and 0.530°C respectively. The estimates for each of the 3 cases fall within

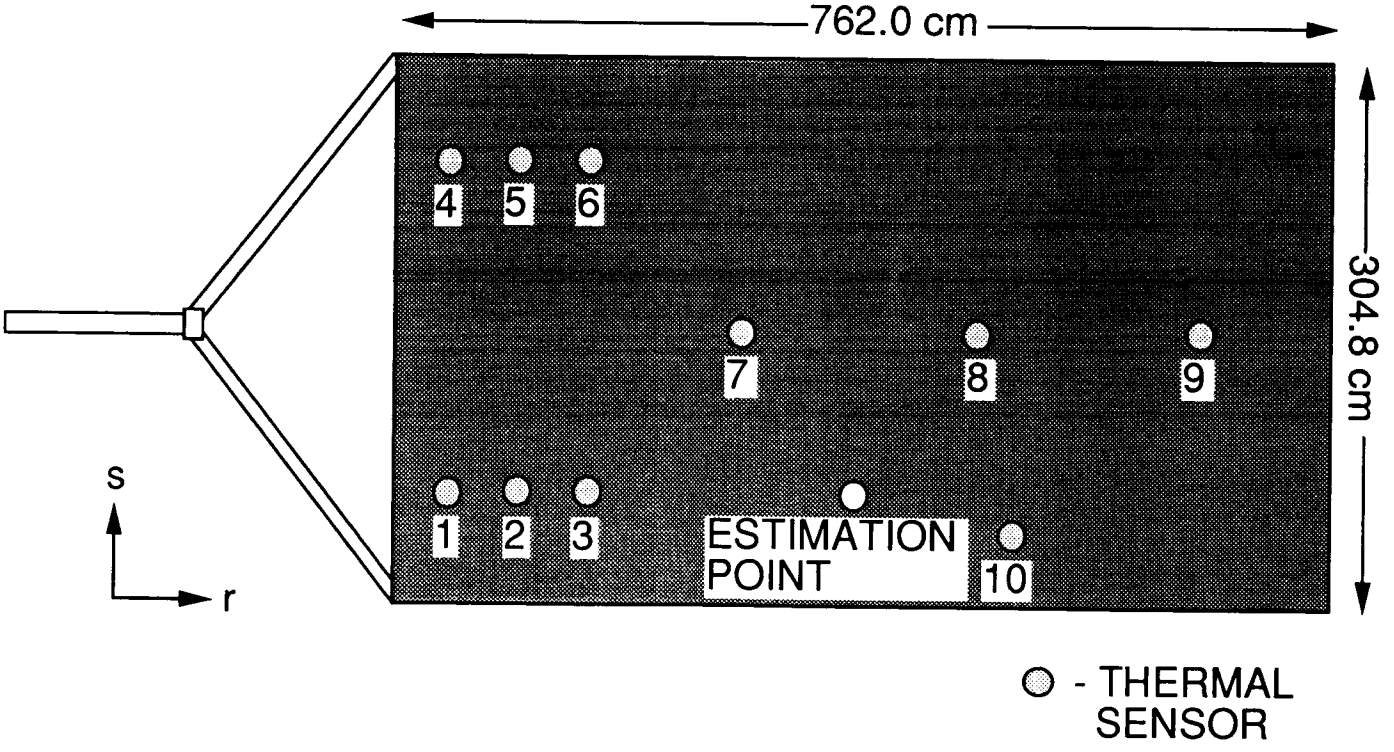

Figure 7: 10-Element Distributed Thermal Sensor Network on a Typical Solar Array (Front Surface)

the range of the observed data with Case 2 exhibiting the largest standard deviation. The standard deviation for Case 2 is a result of the large variance associated with the simulated thermister data set.

If the parameter γ is allowed to approach 0 from its maximum value of 5.0, the quality of the observations is degraded. Furthermore, as γ decreases the estimate is expected to degrade with an increase in the standard devation. To test this hypothesis, estimates and standard deviations for the 3 test cases were recomputed for values of γ ranging from 0.1 to 5.0 in 0.1 increments. Figures 5 and 6 show the estimated temperatures and standard deviations, respectively, for the true data (Case 1), the thermister data (Case 2) and the PRT data (Case 3). An inspection of Figure 5 reveals that the temperature estimate for Case 1 remains essentially constant, $72.955°C$, for $\gamma \geq 0.8$. In the range of $\gamma < 0.8$, the Case 1 temperature estimates reach a maximum of $73.185°C$ at $\gamma = 0.2$ and a minimum of $72.92°C$ at $\gamma = 0.4$. The large deviations occur as the elements of the A_{ij} matrix approach small values resulting in an inverse matrix with large components. Case 2 also shows a non-linear change in the temperature estimate for $\gamma < 0.8$ with a minima at $73.155°C$. The estimate reaches an approximate steady state value of $73.19°C$ with a slight downward trend for $\gamma > 3.5$. Case 3 temperature estimates indicate a linear decrease in temperature from $73.7°C$ to $73.4°C$ with a slope of approximately $0.065\frac{°C}{\gamma_{increment}}$ for $\gamma \geq 0.4$. When $\gamma < 0.4$,the slope increases to $-0.33\frac{°C}{\gamma_{increment}}$. The standard deviations for the 3 Cases, as a function of γ, are illustrated in Figure 6. The standard deviation for the true data (Case 1) remains essentially constant with a value of approximately 0.023°. The thermister data set (Case 2) shows a linear decrease in standard deviation from $2.9°C$ to $2.2°C$ with a

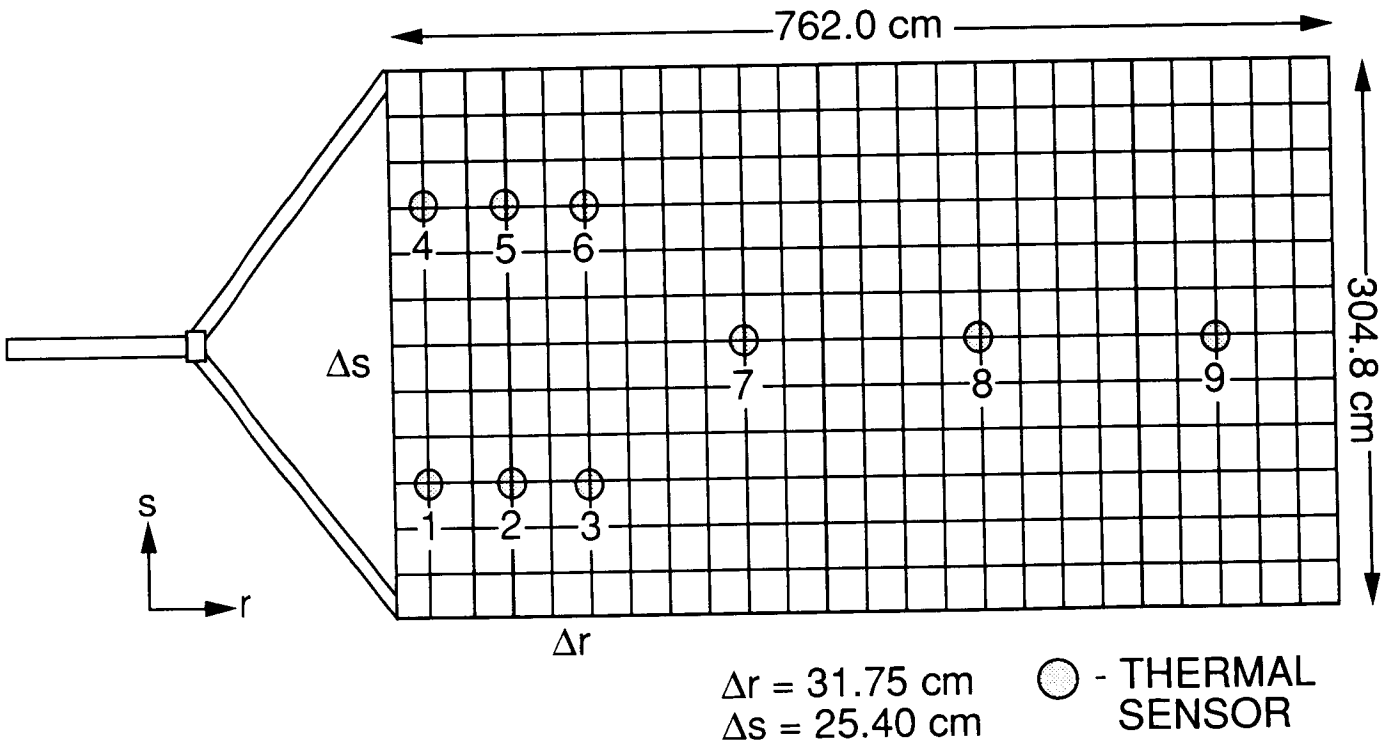

Figure 8: Grid Point Locations Superposed on 9-Element Distributed Thermal Sensor Network

slope of $0.14\frac{^{\circ}C}{\gamma_{increment}}$ as γ increases. The standard deviation of the PRT data also shows a linearly decreasing trend but with a much more subtle slope of $0.04\frac{^{\circ}C}{\gamma_{increment}}$. As expected the estimates for the 3 Cases degrade with an associated increase in the standard deviation as γ approaches a small value.

Another example is illustrated for the case when a hot spot exists on the solar array. For this example a junction box is placed at the location (508,38.1) cm. An additional thermal sensor is also placed at the junction box location. It is assumed that the temperature of the junction box is $82.0^{\circ}C$. Figure 7 shows the new thermal sensor configuration for the front array panel and Table 2 lists the position of the sensors along with the observation data. The parameter γ is equal to 5.0 to provide a maximum correlation of 1.0. The optimal temperature estimation routine provides an estimate of $78.1648^{\circ}C$ and a standard deviation of $1.312^{\circ}C$ for the true temperature, Case 4. Estimates were also computed assuming that the data were measured using a thermister (Case 5) and a PRT (Case 6). The estimates are $75.0298^{\circ}C$ and $77.5123^{\circ}C$ respectively with standard deviations of $2.181^{\circ}C$ and 1.500°. Table 3 summarizes the estimates and the standard deviations for each case.

Since the optimal temperature estimation technique has the ability to provide a temperature estimate at any location, a grid of temperature estimates can be generated to characterize the temperature profile of the entire array using a finite set of data observations. Using only Case 1 from the above discussion this capability will be demonstrated. The grid point locations are illustrated in Figure 8 where the incremental distances between nodes are $\Delta r = 31.75\ cm$ and $\Delta s = 25.4\ cm$. In order to assess the accuracy of the estimation technique, grid points were colocated with the thermal sensor positions as shown in Figure 8. The contoured array front surface temperature profile is shown in Figure 9. The standard deviations associated with the array surface temperature estimates are presented in Figure 10. Table 4 depicts the true and estimated temperatures at the nine thermal sensor locations. A comparison using the percent error between the true and estimated values shows excellent agreement with the largest deviation being 0.309%. The standard deviation for each temperature estimate is also small indicating a small dispersion from the true temperature, thus providing a reasonable estimate for this example.

Table 2: Thermal Sensor Locations and Temperature Measurements for Cases 4-6

Sensor No.	Sensor Position		Temperature $^{\circ}C$		
	r (cm)	s (cm)	Case 4	Case 5 (Thermister)	Case 6 (PRT)
1	31.75	76.2	72.8795	74.4008	72.2307
2	95.25	76.2	72.9475	71.5595	73.5006
3	158.75	76.2	72.9530	71.0906	72.8149
4	31.75	228.6	72.8510	75.2109	73.2364
5	95.25	228.6	72.9433	69.3491	72.4154
6	158.75	228.6	72.9525	76.6270	72.7314
7	285.75	152.4	72.9534	75.1502	73.6916
8	476.25	152.4	72.9534	75.2135	72.6657
9	666.75	152.4	72.9534	75.0416	72.4325
10	508.00	38.1	82.0000	79.8574	82.2281

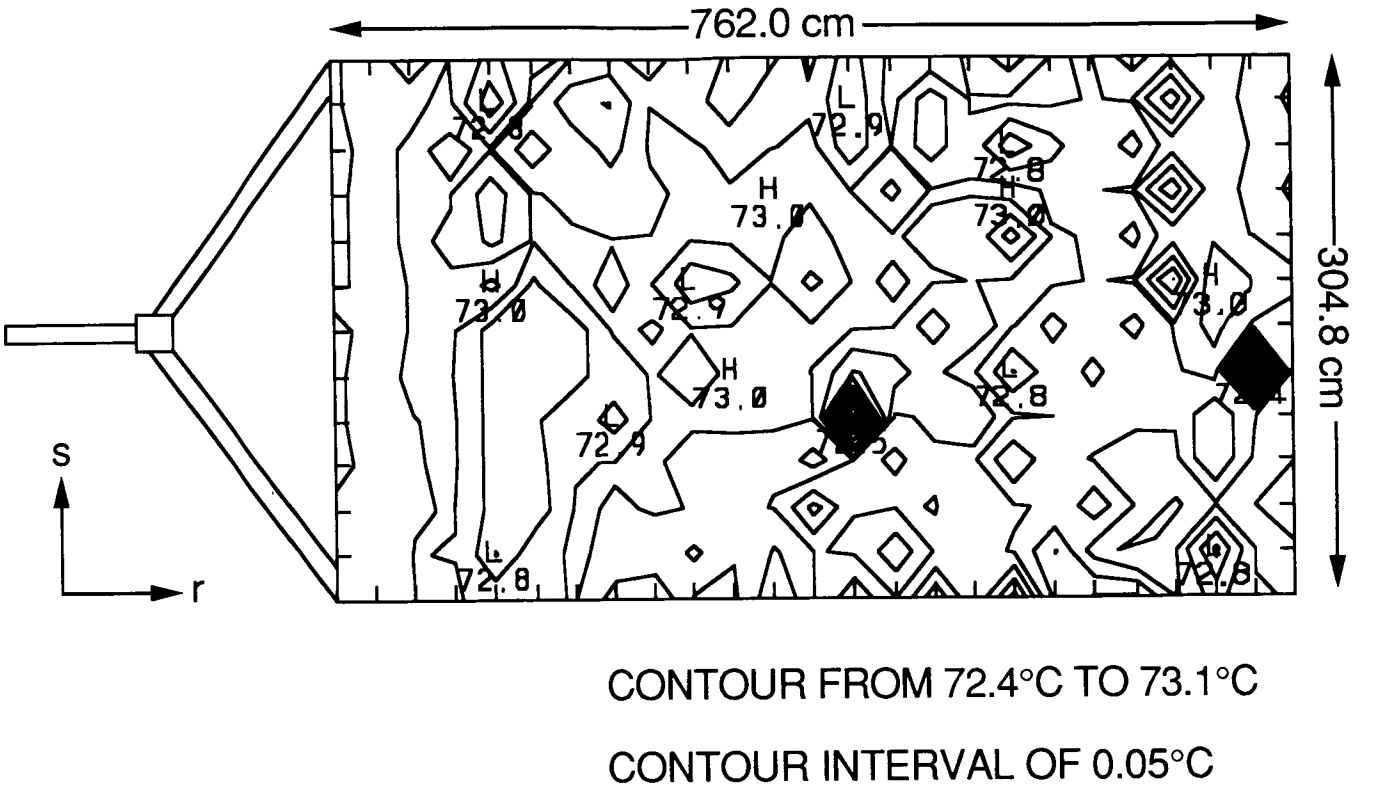

Figure 9: Contoured Array Front Surface Temperature Estimates for 9-Element Distributed Thermal Sensor Network

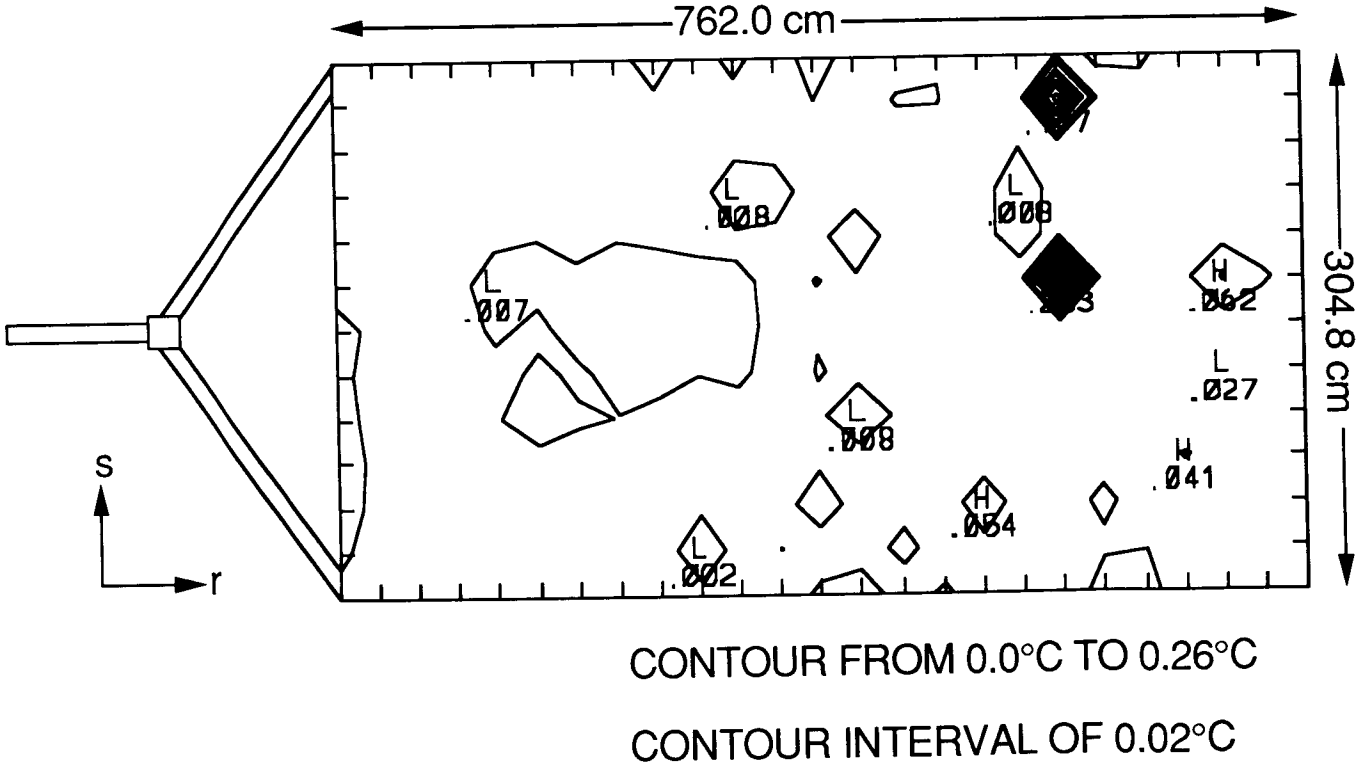

Figure 10: Contoured Standard Deviations Associated with Array Front Surface Temperature Estimates for 9-Element Distributed Thermal Sensor Network

Table 3: Summary of Temperature Estimates and Standard Deviations for Cases 1

Case No.	Temperature Estimate $^{\circ}C$	Standard Deviation $^{\circ}C$
1	72.9523	0.023
2	73.1893	2.205
3	73.0396	0.530
4	78.1648	1.312
5	75.0298	2.181
6	77.5123	1.500

Table 4: Accuracy of Temperature Estimates Compared to True Observations

Sensor No.	Temperature True $^{\circ}C$	Temperature Estimate $^{\circ}C$	Standard Deviation $^{\circ}C$	% Error
1	72.8795	72.8092	0.026	0.096
2	72.9475	72.7262	0.023	0.303
3	72.9530	73.0036	0.022	0.069
4	72.8510	72.8480	0.026	0.004
5	72.9433	72.8636	0.024	0.109
6	72.9525	72.7269	0.022	0.309
7	72.9534	72.8073	0.018	0.200
8	72.9534	72.9120	0.029	0.057
9	72.9534	72.9622	0.033	0.012

CONCLUSIONS

An optimal temperature estimation technique has been described and used to estimate the surface temperature of a satellite solar array at a prescribed location. The technique also provides error information relative to the estimated variable. This technique is capable of determining array surface temperatures at any location, with reasonable accuracy, from a finite set of observational data. Applying the procedure to both surfaces of the array, as a function of time, and differencing the surface temperature estimates will result in an estimated thermal gradient profile. The thermal gradient estimates can then be utilized to drive the TES disturbance model in order to evaluate the true nature of the TES disturbance.

REFERENCES

1. Anonymous, LANDSAT-4 Flight Evaluation Report, 16 October 1982 to 16 January 1983, GE Document 83SDS4203, 16 January 1983, (Contract NAS 5-25300).

2. Bretherton, F.P., R.E. Davis and C.B. Fandry, "A Technique for Objective Analysis and Design of Oceanographic Experiments Applied to MODE-73," *Deep Sea Research*, Vol. 23, pp. 559-582, 1976.

3. Dennehy, C.J., T. Kia and R.V. Welch,"Attitude Determination and Control Subsystem for the TOPEX Satellite," *AIAA Paper* 88-4129, 1988.

4. Dennehy, C., D. Zimbelman and R. Welch,"Sunrise/Sunset Thermal Shock Disturbance Analysis and Simulation for the TOPEX Satellite," *AIAA Paper* 90-0470, 1990.

5. Hamsath, N., and P. M. Bainum,"The Development of an Environmental Disturbance Model for Large Space Structures after the Onset of Thermal Shock," *AIAA Paper* 86-2123, 1986.

6. Liebelt, P.B., *An Introduction to Optimal Estimation*, Addison-Wesley Publishing Company, Massachusetts, 1967.

7. Vigneron, F.R. and R.A. Millar,"Flight Performance of the Stabilization System of the Communications Technology Satellite," *Journal of Guidance and Control*, Vol. 1, 1978, pp. 404-412.